J. Phys. Chem. B XXXX, xxx, 000 A Coarse-Grained Potential Models for Phenyl-Based Molecules: II. Application to Fullerenes

6 AUTHORS, INCLUDING:

Chi-Cheng Chiu
Argonne National Laboratory
34 PUBLICATIONS 430 CITATIONS

SEE PROFILE

Wataru Shinoda
Nagoya University
108 PUBLICATIONS 2,267 CITATIONS

SEE PROFILE

Preston B Moore
University of the Sciences in Philadelphia
73 PUBLICATIONS 2,789 CITATIONS

SEE PROFILE

Steven O Nielsen
University of Texas at Dallas
52 PUBLICATIONS 913 CITATIONS

SEE PROFILE

Coarse-Grained Potential Models for Phenyl-Based Molecules: II. Application to Fullerenes

Chi-cheng Chiu,[†] Russell DeVane,[‡] Michael L. Klein,[‡] Wataru Shinoda,[§] Preston B. Moore,[⊥] and Steven O. Nielsen*,[†]

Department of Chemistry, The University of Texas at Dallas, 800 West Campbell Road, Richardson, Texas 75080, Institute for Computational Molecular Science and Department of Chemistry, Temple University, 1901 North 13th Street, Philadelphia, Pennsylvania 19122, Research Institute for Computational Sciences, National Institute of Advanced Industrial Science and Technology (AIST), Central 2, 1-1-1, Umezono, Tsukuba, Ibaraki 305-8568, Japan, and Department of Chemistry & Biochemistry, University of the Sciences in Philadelphia, 600 South 43rd Street, Philadelphia, Pennsylvania 19104

The interaction of fullerenes with biological systems and the environment is a topic of current interest. Coarse-grained molecular dynamics (CGMD) simulations are well-suited to investigate some of the factors involved because they provide access to time and length scales that are not accessible using fully atomistic simulation methods. In the case of buckyballs (C_{60}) and single-walled carbon nanotubes (SWNTs), it is necessary to parametrize a CG force field that accurately captures the balance between fullerene−fullerene and fullerene−solvent interactions. Herein, we derive CG force field parameters for C_{60} and SWNTs by using the optimized benzene parameters from part I [DeVane, R.; Chiu, C.-c.; Nielsen, S. O.; Shinoda, W.; Moore, P. B.; Klein, M. L. *J. Phys. Chem. B* **2010**, doi: 10.1021/jp9117369]. Solubility, transfer free energy, and dimerization free-energy data for C_{60} and SWNTs obtained using the proposed models show excellent agreement with experimental and fully atomistic MD data. In particular, cluster analysis of C_{60} aggregation in a hydrocarbon melt corroborates the force field parameters. The aggregation behavior of the present CG force field differs considerably from that of models currently in widespread use. The combined results provide a strong basis for applying this model for further large-scale MD studies involving C_{60} and SWNTs.

I. Introduction

Fullerenes and carbon nanotubes have received considerable attention as a result of their unique physical and chemical properties, which open up a broad range of potential applications.[1−4] Recently, much effort has been put forth to investigate nanomaterials as potential drug-delivery and therapeutic agents.[5−12] The success of these applications depends on the ability of these materials to penetrate or cross cellular membranes and the ability to target specific cells or cellular components. The solubility of a molecule in water and oil can often be used as a predictor for the biological activity. For example, the lipid solubility of a species is often highly correlated with its biological activity.[13,14] For nanomaterials, the situation may be more complicated. Some studies have indicated that penetration of cell membranes is accomplished by endocytosis,[6,10] while other studies have suggested insertion and diffusion through the cell membrane.[8,9,11] Regardless, the fundamental partitioning behavior of nanomaterials in membranes and membrane models is an important point of interest and has received considerable attention.[15]

To this end, computer simulations represent a means to investigate the partitioning behavior of nanomaterials in a controlled manner. The resulting data can be used to gain insight into realistic nanoscale phenomena. For example, Li et al.[16] showed from atomistic molecular dynamics (AA MD) studies

that the dispersion interaction between C_{60} and water is so strong that there is a repulsive solvent-induced contribution to the fullerene dimerization free energy, which results in a behavior quite different than that given by the conventional picture of hydrophobic hydration and hydrophobic interactions based on the cavity solute model.[17] However, the use of computer simulations as a predictive tool requires the availability of reliable and validated interaction potentials. Crucially, the entire force field must be determined in a consistent manner to ensure that the delicate balance between water−water, carbon−water, and carbon−carbon interactions translates into validated system properties such as wetting and solubility.[18]

In a recent letter, Maciel et al.[19] point out that despite the availability of a diverse set of AA parameters for the simulation of C_{60} in a biological environment, almost no thermodynamic assessment and validation of these parameters has been realized. Maciel et al. conclude by recommending the use of experimental free-energy data to validate AA fullerene force fields. Indeed, earlier, we advocated this approach for the construction of coarse-grain (CG) force fields, beginning with the work of Nielsen et al.,[20] who developed a CG model for *n*-alkanes using experimental surface tension and bulk density data. More recently, this approach was applied to develop CG parameters for PEG surfactants and amino acids.[21−24]

CG models provide a means to expand the utility of existing computational resources by allowing the exploration of far greater temporal and spatial scales than is possible with traditional AA MD simulations. Recently, Wong-Ekkabut et al.[26] conducted CGMD studies using the MARTINI force field and reported that C_{60} is completely miscible in the hydrocarbon interior of a lipid bilayer; they reported that no fullerene

---

* To whom correspondence should be addressed. E-mail: steven.nielsen@utdallas.edu.
  [†] The University of Texas at Dallas.
  [‡] Temple University.
  [§] National Institute of Advanced Industrial Science and Technology (AIST).
  [⊥] University of the Sciences in Philadelphia.

Application to Fullerenes

J. Phys. Chem. B, Vol. 114, No. 19, 2010 **6395**

aggregates formed in the bilayer membrane even at very high concentration (128 C_{60} molecules in a 1152 molecule lipid bilayer; temperature of 300 K). These findings are surprising given that the solubility of C_{60} in hydrocarbon is low, 3.25×10^{-5} and 2.90×10^{-5} mole fraction in dodecane at 298 and 303 K, respectively.[27] This difference in solubility could result from the structured lipidic environment compared with an isotropic alkane melt[37] or could be due to the deficiencies of the MARTINI force field that have recently been noticed.[28]

In view of the deficiencies of the existing CG force field, the aim of the present study is to explore the utility of a recently developed CG force field[29] for the modeling of fullerenes and to validate the resulting force field against fully AA simulations and experimental data. The methodology for construction and validation of the CG models of C_{60} and single-walled carbon nanotubes (SWNTs) will be presented in section II. Comparison to AA MD and experimental data will be shown in section III. The summary of the present work will appear in section IV.

II. Methods

A. C_{60} Model. We chose to represent a C_{60} molecule using the coarse-grained (CG) benzene site, denoted as BER, developed by DeVane et al.[29] The parametrization of this site was accomplished through the use of experimental thermodynamic and AA MD simulation data and was validated for a range of phenyl-based molecules. Following the CG/AA carbon mapping ratio of 2:3 for the BER site, a CG C_{60} molecule should contain 40 interaction sites. We thus placed 40 BER beads on the surface of a sphere and relaxed the system through energy minimization constrained to the spherical surface. The resulting energy-minimized structure was subsequently treated as a rigid body in the MD studies using the rigid module in LAMMPS; the use of a rigid body description precludes bond and angle potentials.[36] The radius of the sphere determines how far apart these 40 sites are from each other. A smaller radius corresponds to a higher BER density, which in turn results in increased C_{60}-solvent interactions and a strongly increased C_{60}-C_{60} interaction. The dimerization free energies of C_{60} in different solvents compared with AAMD results were used to arrive at the choice of the CG C_{60} radius of 3.5 Å. The resulting C_{60} structure is not perfectly symmetric. Nonetheless, the structural asymmetry is insignificant (see Supporting Information).

To validate this C_{60} CG model, we tested it against AAMD and experimental free-energy data. We first evaluated the transfer free energy from water to heptane ($\Delta G_{Wt-Hept}$). However, since the solvation free energy of C_{60} in water is very low and not well-characterized experimentally, we chose to compare the CG $\Delta G_{Wt-Hept}$ value with results from the CHARMM PARAM27 force field.

We also compared the transfer free energy of our CG C_{60} molecule from heptane to benzene ($\Delta G_{Hept-Benz}$) to experimental data. Since the two hydrocarbon phases are miscible, $\Delta G_{Hept-Benz}$ was evaluated using a thermodynamic cycle by subtracting the transfer free energies from water to heptane ($\Delta G_{Wt-Hept}$) and water to benzene ($\Delta G_{Wt-Benz}$) as shown in Figure 1. The resulting $\Delta G_{Hept-Benz}$ was then compared with the experimental values from Marcus et al.[27]

The dimerization free-energy profiles of C_{60} in water ($\Delta G_{Dimer(Wt)}$) and tridecane ($\Delta G_{Dimer(Tridec)}$) were calculated by using the center-of-mass distance between two C_{60} molecules as the reaction coordinate. These quantities were then compared to the reported AAMD results from Li et al.[16,37] through the use of the "g3data" data extraction tool.[35]

Finally, to directly assess the miscibility of the C_{60} CG model in bulk hydrocarbons, we performed three independent equi-
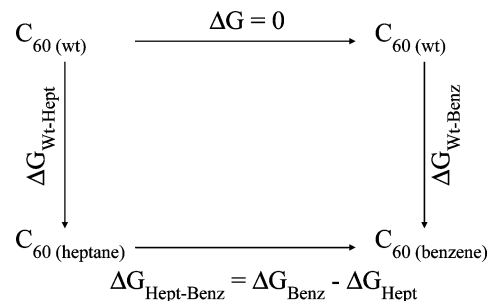

Figure 1. Thermodynamic cycle used to calculate the heptane−benzene transfer free energy of a C_{60} molecule. Water was used as the reference phase in the cycle, and $\Delta G_{Wt-Hept}$ and $\Delta G_{Wt-Benz}$ were calculated separately. The desired $\Delta G_{Hept-Benz}$ was evaluated by subtracting $\Delta G_{Wt-Hept}$ from $\Delta G_{Wt-Benz}$.

librium MD simulations containing 40 C_{60} molecules initially randomly dispersed in 4000 tridecane molecules. These systems were simulated at 1 atm and 310 K for 200 ns.

B. Carbon Nanotube Model. The CG/AA carbon mapping ratio of the BER site is 2:3. Hence, the number of interaction sites per unit area for one CG graphene layer is reduced by a factor of 1.5 from its atomic counterpart, and the bond length between interaction sites is correspondingly magnified by a factor of $(1.5)^{1/2}$. A SWNT can be viewed as a graphene sheet seamlessly rolled into a cylinder; thus, the CG SWNT model constructed from BER sites has a bond length of

$$b_{CG} = \sqrt{1.5} \times b_{AA} \tag{1}$$

where $b_{AA} = 1.422$ Å is the AA aromatic carbon−carbon bond length. The resulting CG bond length is thus $b_{CG} = 1.742$ Å. The properties of individual SWNTs are uniquely determined by the chiral vector (n,m), which determines the rolling direction of the graphene sheet and is perpendicular to the SWNT long axis.[38] The chiral vector of the CG SWNT can be related to that of the AA SWNT by

$$(n_{CG}, m_{CG}) = \left(\frac{n_{AA}}{\sqrt{1.5}}, \frac{m_{AA}}{\sqrt{1.5}}\right) \tag{2}$$

Due to the noninteger factor, the CG SWNT can only correspond approximately to a particular AA SWNT. We can choose a similar size or a similar chirality. For instance, an (8,8) CG SWNT with a 13.31 Å diameter is similar to a (10,10) AA SWNT with a 13.58 Å diameter. On the other hand, by choosing a (n_{CG}, m_{CG}) vector with the same n/m ratio as the AA SWNT, we can preserve the chirality of the SWNT.

In this study, the CG SWNTs were aligned with the x-axis of the simulation unit cell and treated as rigid molecules, as previously described for the C_{60} model. The terminal SWNT BER sites at one end of the SWNT were bonded through a periodic image to the BER sites at the other SWNT end, thus creating an infinitely long SWNT. The simulation box was fixed in the x-direction but allowed to change in the y- and z-dimensions for pressure control. To test the SWNT CG model, we calculated the dimerization free energy per unit length in water of a (13,0) CG SWNT with a 12.5 Å diameter, which corresponds to a (16,0) AA SWNT with a 12.5 Å diameter, and compared with the reported AA result[30,31] and theoretical prediction.[39]

C. Molecular Dynamics Simulation. All of the AAMD simulations were carried out using the CHARMM PARAM27 force field parameters[40] using the NAMD simulation code[41] and were analyzed using the VMD visualization tool.[42] The long-range Coulomb interactions were calculated via the particle mesh Ewald method.[43,44] Bonds involving hydrogen atoms were constrained via the SHAKE/RATTLE method.[45] A 2 fs time step was used to integrate the equations of motion. CGMD simulations were performed using the LAMMPS code from the Sandia National Laboratory and extended by us to implement our CG models.[36] All CG simulations were carried out using a two-level RESPA multitime step integrator.[46] The bond and angle potentials were evaluated in the inner time step of 1 fs, and the nonbonded interactions were evaluated in the outer time step of 10 fs. The temperature and the pressure were controlled using the Nosé−Hoover algorithm.[47] The CG models for solvent molecules (water and alkane) were taken from the CG force field developed by Shinoda et al,[21] and the interactions involving the BER site used the parameters developed by DeVane et al.[29] The heptane model was produced by using "CT2" and "CM" CG sites (CT2−CM−CT2); tridecane was modeled using the CT2−CM−CM−CM−CT2 representation.

D. Cluster Analysis. C_{60} molecules were assigned to clusters for data analysis purposes as follows. For a given snapshot of the system coordinates, the centers of mass of the 40 C_{60} molecules were recorded in a list L. An element of this list was moved to list 1, leaving list L with 39 members. Next, the distance D_{L1} between list L and list 1 was identified, where we define the distance D between two lists A and B by

$$D_{AB} = \min_{i \in A, j \in B} d^*(i,j) \qquad (3)$$

where $d(i,j)$ represents the distance between member i of list A and member j of list B and * denotes the minimum image convention. The element i of list L corresponding to D_{L1} is moved to list 1 if $D_{L1} < d_{threshold}$ or else is moved to a new list (called list 2). Next, the distance D_{Lk} is identified for $k \in \{1, 2\}$; let k_* be the list corresponding to the smallest D_{Lk} (if list 2 is empty, $k_* = 1$). The element i of list L corresponding to D_{Lk_*} is moved to list k_* if $D_{Lk_*} < d_{threshold}$ or else is moved to a new list (called list 3 if list 2 is not empty; otherwise called list 2). This procedure is repeated until list L is empty. The resulting lists $\{1, 2, ..., n\}$ correspond to the n clusters in the system. The total number of elements in a list represents the size of that cluster.

A normalized histogram of the cluster size for each equilibrium simulation is recorded as a function of the simulation time using a threshold value of $d_{threshold} = 12$ Å. For example, in Figure 6c, the final state of the system consists of a 12-membered cluster and a 28-membered cluster; these two clusters are each assigned a fractional occupation number of 0.5. The threshold value, $d_{threshold} = 12$ Å, is determined as the first maximum in the dimerization free-energy profile (Figure 5).

E. Free-Energy Calculation. The free-energy calculations for the C_{60} systems were performed using the umbrella sampling technique combined with the weighted histogram analysis method (WHAM).[48] The transfer free-energy calculations had as their initial condition an equilibrated water/oil system (water/heptane or water/benzene) containing one C_{60} molecule with the interface perpendicular to the z-axis of the simulation unit cell. The transfer free-energy profiles were calculated as a function of the z-distance between the C_{60} center of mass and the water slab center of mass. Sampling windows were deployed
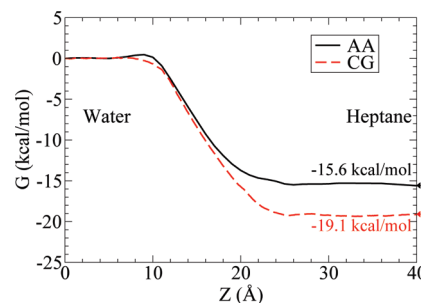

Figure 2. C_{60} water-to-heptane transfer free-energy profiles for both the AA and CG representations. The solid (black) line represents the AAMD result, and the dashed (red) line represents the CGMD result.

every 4 Å in the z-direction, each with an applied harmonic biasing potential of force constant 0.5 kcal/mol/Å². The simulations were run in the NP$_n$AT ensemble at 1 atm and 303 K with the simulation box fixed in the x- and y-dimensions. The C_{60} dimerization free-energy profiles were calculated in the NPT ensemble as a function of the distance between the C_{60} centers of mass using sampling windows placed every 2 Å, each with a harmonic biasing potential of force constant 1.0 kcal/mol/Å².

The CG SWNT dimerization free energy was evaluated based on Jarzynski's equality using steered MD (SMD) as implemented in LAMMPS.[36,49] The reaction coordinate was chosen as the separation distance between the two SWNT long axes. The reaction coordinate varied between 42 Å and the SWNT contact distance of 14 Å. The 32 Å pulling distance was partitioned into 8 separate segments of 4 Å each. The constant velocity pulling speed was 1 Å/ns, and a force constant of 100 kcal/mol/Å² was used for all of the SMD runs. Each segment was sampled with 20 SMD simulations, from which an overall free-energy profile was obtained.

III. Results and Discussion

A. C_{60} Model. As already mentioned, we represent a C_{60} molecule using 40 CG benzene sites, denoted BER.[29] The parametrization of the intermolecular potentials for this site was accomplished through the use of experimental thermodynamic data and was validated for a range of phenyl-based molecules. Herein, we validate the BER-based C_{60} CG model by testing it against a host of AAMD and experimental free-energy data. The 40 BER beads were energy-minimized on the surface of a 3.5 Å radius sphere and subsequently treated as a rigid body in the CGMD studies.

B. C_{60} Transfer Free Energy. In a recent letter, Maciel et al.[19] make a strong case for using the transfer free energy of a single C_{60} molecule between different solvents as a stringent means to assess and validate fullerene force fields. We validate our CG C_{60} model against both fully AAMD and experimental data as follows.

The C_{60} water-to-heptane transfer free energy is evaluated using umbrella sampling. The resulting free-energy profiles are shown in Figure 2 for both the AA and CG models. We obtain $\Delta G_{Wt-Hept} = -19.1$ kcal/mol for the CG model, which is relatively close to the AA result of -15.6 kcal/mol. This value is very reasonable, as discussed in the context of C_{60} water-to-lipid bilayer partitioning by Bedrov et al.[32] and D'Rozario et al.[25] Moreover, the width of the interfacial region is very similar for the two profiles, indicating that C_{60} experiences the same effective interaction range.

The C_{60} heptane-to-benzene transfer free energy must be evaluated using a thermodynamic cycle because the two

Application to Fullerenes

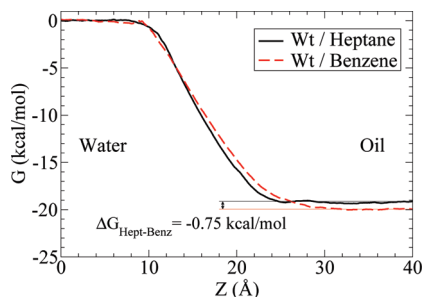*J. Phys. Chem. B, Vol. 114, No. 19, 2010* **6397**

Figure 3. The C_{60} water-to-heptane and water-to-benzene transfer free-energy profiles used to calculate the C_{60} heptane-to-benzene transfer free energy of the CG model. The solid (black) line represents the free-energy profile from water to heptane, and the dashed (red) line represents that from water to benzene. The net result of $\Delta G_{Hept-Benz} = -0.75$ kcal/mol is calculated from the thermodynamic cycle shown in Figure 1.
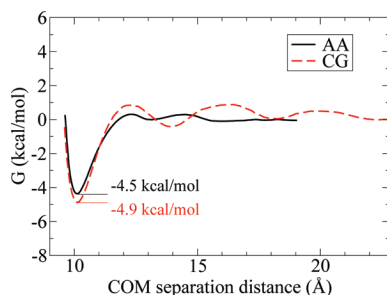

Figure 4. The free-energy profile of the dimerization of C_{60} in water is shown for both the AA and CG representations. The solid (black) line represents the AAMD result from Li et al.,[16] and the dashed (red) line represents the result using the CG representation.

hydrocarbon phases are miscible. We chose to use water in the thermodynamic cycle, as shown in Figure 1. The two free-energy profiles used to compute $\Delta G_{Hept-Benz}$ are the C_{60} transfer free energy from water to heptane ($\Delta G_{Wt-Hept}$) and that from water to benzene ($\Delta G_{Wt-Benz}$), as shown in Figure 3. Following the thermodynamic cycle, $\Delta G_{Hept-Benz}$ was computed by subtracting $\Delta G_{Wt-Hept}$ from $\Delta G_{Wt-Benz}$. We obtained $\Delta G_{Hept-Benz} = -0.75$ kcal/mol, which is in excellent agreement with the experimental value of -0.7 kcal/mol.[27]

C. C_{60} Dimerization Free Energy. The dimerization free energy of C_{60} in water at 298 K under the CG representation is compared with the reported AA result,[16,33] as illustrated in Figure 4. We obtain $\Delta G_{Dimer(Wt)} = -4.9$ kcal/mol for the CG model, which agrees well with the AA value of -4.5 kcal/mol.[16] The barriers in the free-energy profile correspond to structured water layers between the two C_{60} molecules. The wider free-energy barriers in the CG system are the consequence of a larger solvent bead size resulting from the mapping of three AA water molecules into one CG water interaction site. In addition, the CG free-energy profile shows longer-range undulations than the AA model. These undulations are a result of a compromise in the CG representation of water between matching the AA water–water pair correlation function and matching the experimental compressibility of water. Our CG water model has too much structure, which is an inevitable consequence of coarse-graining.[21] However, the close match between $\Delta G_{Dimer(Wt)}$ for the CG and AA representations ensures that the CG force field has the correct balance between C_{60}–C_{60} and C_{60}–water interactions.

Figure 5 shows the dimerization free-energy profiles of C_{60} in tridecane at 310 K for the CG model and the reported AA results.[37] We obtain $\Delta G_{Dimer(Tridec)} = -2.1$ kcal/mol for the CG model, which is close to the AA result of -1.7 kcal/mol. As
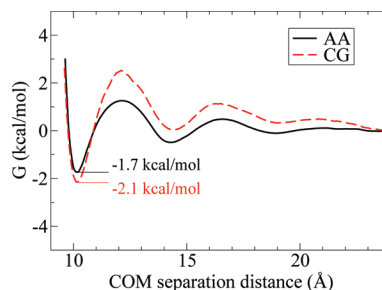

Figure 5. The free-energy profile of the dimerization of C_{60} in tridecane is shown for both the AA and CG representations. The solid (black) line represents the AAMD result from Li et al.,[37] and the dashed (red) line represents the result using the CG representation.

found for the dimerization in water, the free-energy profile has barriers corresponding to the layers of alkane between the C_{60} molecules. However, unlike in water, the barrier positions are identical for the CG and AA representations. Although the barrier heights are different, they are within ~2 kcal/mol of each other. The excellent agreement between the CG and AA free-energy profiles suggests that the CG force field has the correct balance between C_{60}–C_{60} and C_{60}–alkane interactions.

D. C_{60} Miscibility in Hydrocarbon. To directly study the miscibility of C_{60} in bulk hydrocarbon under the CG force field, we conducted 3 independent equilibrium MD simulations starting with 40 C_{60} molecules individually dispersed in 4000 tridecane molecules. The behavior of the C_{60} molecules was monitored by performing a cluster analysis on their centers of mass as described in the Methods section. The resulting data are shown in Figure 6 in the form of a cluster fractional occupation number distribution. For a given elapsed simulation time, the cluster sizes are shown shaded by their fractional occupation number. Initially, the cluster size of one has a fractional occupation number of 1.0 since each C_{60} occupies its own cluster. From this initial condition, C_{60} molecules begin to aggregate with each other. Large-sized clusters are increasingly populated at the expense of small-sized clusters as the simulation progresses. The time scale over which the distributions of Figure 6 change slows down as the total number of clusters decreases because the average distance between two clusters increases; the time scale is governed largely by diffusion. After 200 ns of simulation time, we find the 40 C_{60} molecules grouped into either 2 (system c) or 3 (systems a and b) clusters. Figure 7 shows snapshots of the C_{60} molecules corresponding to the marked time values in Figure 6c. The final state of the system consists of a 12-membered cluster and a 28-membered cluster. We established in Figure 5 that the C_{60} dimerization free energy in hydrocarbons is weak. Nonetheless, the data shown in Figure 7 strongly suggest that all three 40 C_{60} systems will completely phase separate on a longer time scale. This is consistent with experimental data where a solubility of 3×10^{-5} mole fraction implies that we would need to use an order of magnitude larger number of hydrocarbon molecules to solubilize even one C_{60} molecule.[27] This behavior would seem to be at odds with the findings of Wong-Ekkabut et al.,[26] who showed that C_{60} is completely miscible in the hydrocarbon interior of a lipid bilayer. Aside from the difference in force fields, the discrepancy in miscibility of C_{60} in a hydrocarbon solvent could be due to the structured lipidic environment versus an isotropic alkane melt, as suggested by Li et al.[37]

E. SWNT Model. We chose to represent a SWNT using the same CG benzene sites, denoted BER, as in the C_{60} model discussed above. Since the CG/AA carbon mapping ratio of the BER site is 2:3, the bond length between interaction sites is
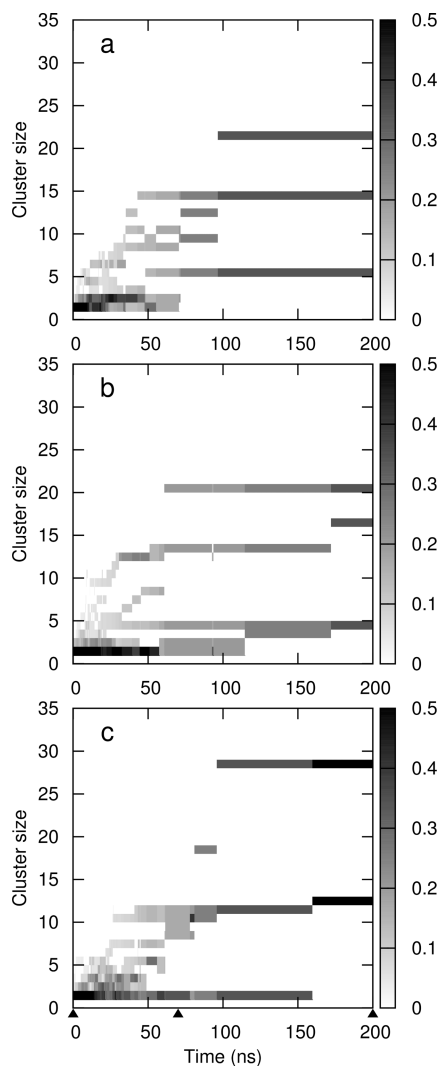
Figure 6. The time evolution of the cluster fractional occupation number distribution for three independent MD simulations (labeled a, b, and c). Each panel represents a 200 ns MD simulation of a system with 40 C_{60} molecules initially individually dispersed in 4000 tridecane molecules. A darker shading represents a higher fractional occupation number. Note that fractional occupation numbers from 0.5 to 1 appear as the darkest shade. The marked (▲) time values in panel c correspond to the snapshots in Figure 7.

magnified by a factor of $(1.5)^{1/2}$, and the chiral (n,m) vector of the CG SWNT is reduced by a factor of $(1.5)^{1/2}$ in both n and m. Due to this noninteger factor, the CG SWNT can only correspond approximately to a particular AA SWNT. To validate the CG fullerene model, we calculated the dimerization free energy per unit length in water of a (13,0) CG SWNT with a 12.5 Å diameter, which corresponds to a (16,0) AA SWNT with a 12.5 Å diameter.

F. SWNT Dimerization Free Energy. Figure 8 displays the dimerization free energy per unit length in water of two (13,0) CG SWNTs, which correspond to two (16,0) AA SWNTs as discussed above. The minimum of the free energy has a value of −2.5 kcal/mol/Å. According to Walther et al., the AA (16,0) SWNT has a dimerization free energy of −4.1 kcal/mol/Å.[30] In addition, Lum et al. calculated a free energy per unit length of −5.5 kcal/mol/Å through a theoretical analysis of water interacting with four parallel cylinders, each 12 Å in diameter, which gives a lower bound of −2.75 kcal/mol/Å for the dimerization free energy. These AA MD and theoretical results are in reasonable agreement with our CG model. The data
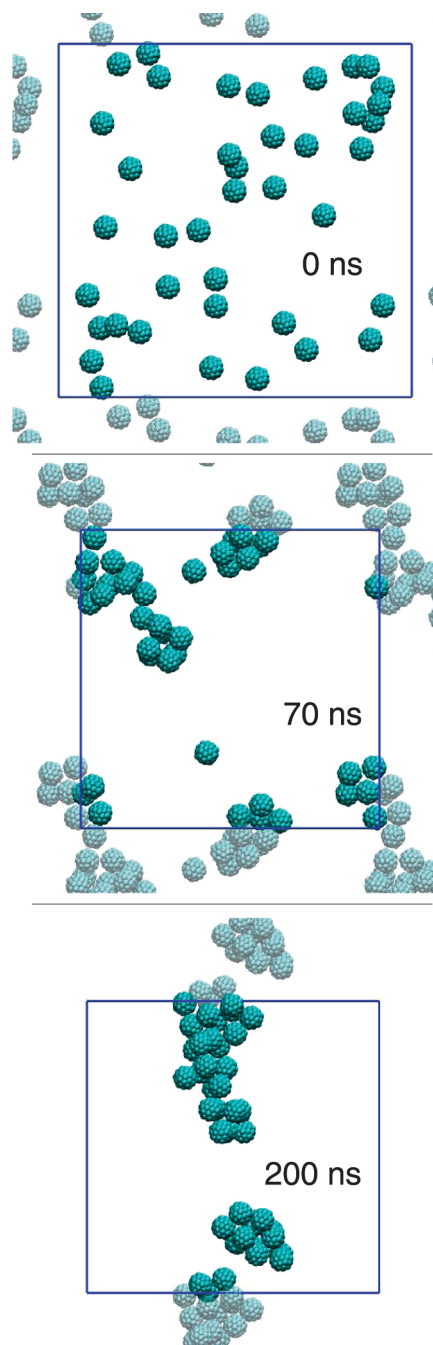

Figure 7. Snapshots of a MD simulation of 40 C_{60} molecules initially individually dispersed in 4000 tridecane molecules. These snapshots correspond to the marked time values in Figure 6c. C_{60} molecules in the simulation unit cell are shown in an opaque representation, whereas molecules belonging to periodic images are shown in a transparent representation.

includes a repulsive solvent-induced contribution to the dimerization free energy,[16] which results in a qualitatively different behavior than that based on the cavity solute model.[17] The solvent-induced interaction is calculated by subtracting the dimerization free energy in vacuum (data not shown) from that obtained in water. As shown in Figure 8, water induces a repulsive interaction between the SWNTs, which agrees with the MD result reported by Li et al.[31] The long-range free-energy barriers in the dimerization free energy are mainly contributions from water. Like the C_{60} dimerization in water, the CG water structures around the SWNT into layers, causing undulating free-energy barriers as two SWNTs approach each other.
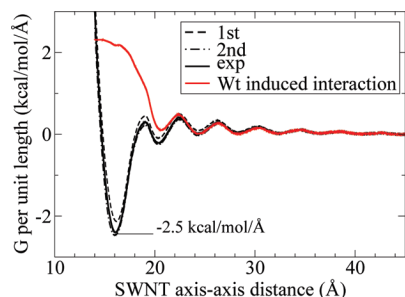
Application to Fullerenes

J. Phys. Chem. B, Vol. 114, No. 19, 2010 **6399**

Figure 8. The free-energy profile per unit length for the dimerization of (13,0) CG SWNTs in water calculated using steered MD. The dashed black, dot−dashed black, and solid black lines represent the first-order cumulant, the second-order cumulant, and the full exponential estimates, respectively. The overlap of the second-order and full exponential estimates indicates a Gaussian distribution of work values. The red solid line is the water-induced interaction calculated by subtracting the dimerization free energy in vacuum (data not shown) from that obtained in water.

These long-range free-energy barriers are not seen in the AA free-energy profile[30,31] but are unavoidable in the current CG model. The total dimerization free energy is given by the free-energy values per unit length presented here (Figure 8) multiplied by the nanotube length. Hence, the total free-energy change can be very large, suggesting a strong tendency in the CG model for aqueous SWNTs to form self-contacts. This result is in accord with the special solvents required to suspend SWNTs in water. Solvents used include surfactants such as sodium dodecyl sulfate and alkyl benzene sulfonates as well as DNA and proteins.[12,50]

IV. Conclusions

In this study, we presented coarse-grained (CG) models for C_{60} and single-walled carbon nanotubes (SWNTs) by applying the BER interaction site from our CG phenyl-based force field. We validated the resulting fullerene force field against a range of fully AA and experimental data. Specifically, the CG C_{60} transfer free energies between water and heptane and between heptane and benzene were computed and compared to fully AA and experimental solubility data, respectively. The solubility of C_{60} in hydrocarbon was probed in greater detail through the use of large-scale simulations of initially individually dispersed C_{60} molecules. The resulting C_{60} aggregation behavior was consistent with experimental solubility data and suggests that $>10^4$ solvent molecules are required to observe any miscibility. The CG C_{60} dimerization free energy in water and that in hydrocarbons were computed and compared to fully AA data. Finally, the CG SWNT dimerization free energy in water was computed and compared to fully AA and theoretical data. The CG model agrees with the AA data of Li et al.[16] showing a repulsive solvent-induced contribution to the dimerization free energy. Longer-range structure is seen in the CG dimerization free-energy profiles in water for both C_{60} and SWNT as compared to AA simulation data. These artificial barriers are the result of a compromise in the CG representation of water between matching the AA water−water pair correlation function and matching the experimental compressibility of water.[21] Note the CG representations of C_{60} and SWNTs use the BER site, which was optimized for small phenyl-based molecules. This leads to the small discrepancy in the free-energy data between the CG and AA models in this study. Better agreement could be achieved by additional tuning of the BER interaction parameters, but this would require a rebalancing of the entire

CG force field. The CG fullerene force field described herein represents an improvement over the existing CG models in the literature. The validated force field provides a strong basis for applying the model for further large-scale MD studies such as the interaction of fullerenes with lipid bilayers and proteins.[34]

Supporting Information Available: Quantification of the implication of CG C_{60} asymmetry is included. This material is available free of charge via the Internet at http://pubs.acs.org.

References and Notes

(1) Frank, S.; Poncharal, P.; Wang, Z. L.; de Heer, W. A. *Science* **1998**, *280*, 1744.

(2) Liu, C.; Fan, Y. Y.; Liu, M.; Cong, H. T.; Cheng, H. M.; Dresselhaus, M. S. *Science* **1999**, *286*, 1127.

(3) Langer, R. *Science* **1990**, *249*, 1527.

(4) Wu, H. Q.; Wei, X. W.; Shao, M. W.; Gu, J. S.; Yu, M. Z. *J. Mater. Chem.* **2002**, *12*, 919.

(5) Ruthrotha Selvi, B.; Jagadeesan, D.; Suma, B. S.; Nagashankar, G.; Arif, M.; Balasubramanyam, K.; Eswaramoorthy, M.; Kundu., T. K. *Nano Lett.* **2008**, *8*, 3182.

(6) Kam, N. W. S.; Jessop, T. C.; Wender, P. A.; Dai, H. J. *J. Am. Chem. Soc.* **2004**, *126*, 6850.

(7) Kam, N. W. S.; Dai, H. J. *J. Am. Chem. Soc.* **2005**, *127*, 6021.

(8) Pantarotto, D.; Briand, J.; Prato, M.; Bianco, A. *Chem. Commun.* **2004**, *1*, 16.

(9) Lu, Q.; Moore, J. M.; Huang, G.; Mount, A. S.; Rao, A. M.; Larcom, L. L.; Ke, P. C. *Nano Lett.* **2004**, *4*, 2473.

(10) Cherukuri, P.; Bachilo, S. M.; Litovsky, S. H.; Weisman, R. B. *J. Am. Chem. Soc.* **2004**, *126*, 15638.

(11) Bianco, A.; Hoebeke, J.; Godefroy, S.; Chaloin, O.; Pantarotto, D.; Briand, J.-P.; Muller, S.; Prato, M.; Partidos, C. D. *J. Am. Chem. Soc.* **2005**, *127*, 58.

(12) Sayes, C. M.; Liang, F.; Hudson, J. L.; Mendez, J.; Guo, W.; Beach, J. M.; Moore, V. C.; Doyle, C. D.; West, J. L.; Billups, W. E.; Ausman, K. D.; Colvin, V. L. *Toxicol. Lett.* **2006**, *16*, 135.

(13) Levitan, H. *Proc. Natl. Acad. Sci. U.S.A.* **1977**, *74*, 2914–2918.

(14) Gulden, M.; Morchel, S.; Seibert, H. *Toxicology in Vitro* **2001**, *15*, 233–243.

(15) Lyon, D. Y.; Adams, L. K.; Falkner, J. C.; Alvarez, P. J. J. *Environ. Sci. Technol.* **2006**, *40*, 4360–4366.

(16) Li, L.; Bedrov, D.; Smith, G. D. *Phys. Rev. E* **2005**, *71*, 011502.

(17) Chandler, D. *Nature* **2002**, *417*, 491.

(18) Werder, T.; Walther, J. H.; Jaffe, R. L.; Halicioglu, T.; Koumoutsakos, P. *J. Phys. Chem. B* **2003**, *107*, 1345–1352.

(19) Maciel, C.; Fileti, E. E.; Rivelino, R. *J. Phys. Chem. B* **2009**, *113*, 7045–7048.

(20) Nielsen, S. O.; Lopez, C. F.; Srinivas, G.; Klein, M. L. *J. Chem. Phys.* **2003**, *119*, 7043–7049.

(21) Shinoda, W.; DeVane, R.; Klein, M. L. *Mol. Simul.* **2007**, *33*, 27–36.

(22) Shinoda, W.; DeVane, R.; Klein, M. L. *Soft Matter* **2008**, *4*, 2454–2462.

(23) Klein, M. L.; Shinoda, W. *Science* **2008**, *321*, 798–800.

(24) DeVane, R.; Shinoda, W.; Moore, P. B.; Klein, M. L. *J. Chem. Theory Comput.* **2009**, *5*, 2115.

(25) D'Rozario, R. S. G.; Wee, C. L.; Wallace, E. J.; Sansom, M. S. P. *Nanotechnology* **2009**, *20*, 115102.

(26) Wong-Ekkabut, J.; Baoukina, S.; Triampo, W.; Tang, I.-M.; Tieleman, D. P.; Monticelli, L. *Nature Nanotechnol.* **2008**, *3*, 363–368.

(27) Marcus, Y.; Smith, A. L.; Korobov, M. V.; Mirakyan, A. L.; Avramenko, N. V.; Stukalin, E. B. *J. Phys. Chem. B* **2001**, *105*, 2499–2506.

(28) Winger, M.; Trzesniak, D.; Baron, R.; van Gunsteren, W. F. *Phys. Chem. Chem. Phys.* **2009**, *11*, 1934–1941.

(29) DeVane, R.; Chiu, C.-c.; Nielsen, S. O.; Shinoda, W.; Moore, P. B.; Klein, M. L. *J. Phys. Chem. B* **2010**, doi: 10.1021/jp9117369.

(30) Walther, J. H.; Jaffe, R. L.; Kotsalis, E. M.; Werder, T.; Halicioglu, T.; Koumoutsakos, P. *Carbon* **2004**, *42*, 1185–1194.

(31) Li, L.; Bedrov, D.; Smith, G. D. *J. Phys. Chem. B* **2006**, *110*, 10509–10513.

(32) Bedrov, D.; Smith, G. D.; Davande, H.; Li, L. *J. Phys. Chem. B* **2008**, *112*, 2078–2084.

(33) Kim, H.; Bedrov, D.; Smith, G. D. *J. Chem. Theory Comput.* **2008**, *4*, 335–340.

(34) Bakry, R.; Vallant, R. M.; Najam-Ul-Haq, M.; Rainer, M.; Szabo, Z.; Huck, C. W.; Bonn, G. K. *Int. J. Nanomed.* **2007**, *2*, 639–649.

(35) g3data Website. http://www.frantz.fi/software/g3data.php (2003).

(36) Plimpton, S. *J. Comput. Phys.* **1995**, *117*, 1–19.

(37) Li, L.; Davande, D.; Bedrov, D.; Smith, G. D. *J. Phys. Chem. B* **2007**, *111*, 4067.

(38) Saito, R.; Dresselhaus, G.; Dresselhaus, M. S. *Physical Properties of Carbon Nanotubes*; Imperial College Press: London, 1998.

(39) Lum, K.; Chandler, D.; Weeks, J. D. *J. Phys. Chem. B* **1999**, *103*, 4570–4577.

(40) MacKerell, A. D.; Bashford, D.; Bellott, M.; Dunbrack, R. L.; Evanseck, J. D.; Field, M. J.; Fischer, S.; Gao, J.; Guo, H.; Ha, S.; Joseph-McCarthy, D.; Kuchnir, L.; Kuczera, K.; Lau, F. T. K.; Mattos, C.; Michnick, S.; Ngo, T.; Nguyen, D. T.; Prodhom, B.; Reiher, W. E.; Roux, B.; Schlenkrich, M.; Smith, J. C.; Stote, R.; Straub, J.; Watanabe, M.; Wiorkiewicz-Kuczera, J.; Yin, D.; Karplus, M. *J. Phys. Chem. B* **1998**, *102*, 3586–3616.

(41) Phillips, J. C.; Braun, R.; Wang, W.; Gumbart, J.; Tajkhorshid, E.; Villa, E.; Chipot, C.; Skeel, R. D.; Kale, L.; Schulten, K. *J. Comput. Chem.* **2005**, *26*, 1781–1802.

(42) Humphrey, W.; Dalke, A.; Schulten, K. *J. Mol. Graphics* **1996**, *14*, 33–38.

(43) Darden, T. A.; York, D. M.; Pedersen, L. G. *J. Chem. Phys.* **1993**, *98*, 10089.

(44) Allen, M. P.; Tildesley, D. J. *Computer Simulations of Liquids*; Oxford Science: New York, 1987.

(45) Ryckaert, J. P.; Ciccotti, G.; Berendsen, H. J. C. *J. Comput. Phys.* **1977**, *23*, 327–341.

(46) Tuckerman, M. E.; Berne, B. J.; Martyna, G. J. *J. Chem. Phys.* **1992**, *97*, 1990.

(47) Hoover, W. G. *Phys. Rev. A* **1985**, *31*, 1695.

(48) Kumar, S.; Bouzida, D.; Swendsen, R. H.; Kollman, P. A.; Rosenberg, J. M. *J. Comput. Chem.* **1992**, *13*, 1011–1021.

(49) Jarzynski, C. *Phys. Rev. Lett.* **1997**, *78*, 2690.

(50) Moore, V. C.; Strano, M. S.; Haroz, E. H.; Hauge, R. H.; Smalley, R. E. *Nano Lett.* **2003**, *3*, 1379.